Crystal Structure and Cation Disorder in Bulk Cu_2ZnSnS_4 Using Neutron Diffraction and X-Ray Anomalous Scattering

C.J. Bosson[1], M.T. Birch[1], D.P. Halliday[1], K.S. Knight[2], C.C. Tang[3], A.K. Kleppe[3], and P.D. Hatton[1]

[1]Department of Physics, The University of Durham, Durham, DH1 3LE, UK
[2]ISIS Neutron and Muon Source, Rutherford Appleton Laboratory, Didcot, OX11 0QX, UK
[3]Diamond Light Source, Harwell Science & Innovation Campus, Didcot, OX11 0DE, UK

***ABSTRACT* — Cu_2ZnSnS_4 (CZTS) is a promising material for the absorber layer in sustainable thin film photovoltaic cells, but its best efficiencies are currently limited by low open-circuit voltages, thought to be due to defects such as disorder between the copper and zinc lattice sites. Samples of CZTS with stoichiometric and Cu-poor, Zn-rich (optimally doped for device application) starting compositions were fabricated by solid state reaction and their crystal structures were investigated using high-resolution neutron diffraction and anomalous scattering synchrotron X-ray diffraction. Both samples were found to be exclusively kesterite with significant mixing of Cu and Zn on the 2*a*, 2*c*, and 2*d* Wyckoff sites but negligible defect presence on the Sn 2*b* or S 8*g* sites. Importantly, the occupancies of the 2*a* and 2*c* sites were found to be identical, meaning the kesterite symmetry is preserved.**

***Index Terms* — anomalous scattering, Cu_2ZnSnS_4, crystal structure, neutron diffraction**

I. Introduction

Solar electricity will be an important contributor to the energy mix of the future. However, many materials currently in use and being investigated for the absorber layer of photovoltaic solar cells, such as silicon, CdTe, and $Cu_2InGaSe_4$ (CIGS), are prohibitively expensive (silicon due to high manufacturing costs; others due to element costs, particularly of Ga, In, and Te); contain elements not abundant enough to contribute electricity on the TW scale needed (particularly Te, Se, and In); are toxic (particularly Cd and Se); or a combination of the above. [1]

Cu_2ZnSnS_4 (CZTS), an intrinsically p-type direct gap semiconductor with near-optimal band gap of 1.4-1.5 eV and high absorption coefficient $>10^4$ cm^{-1}, is a promising absorber material with none of these problems. It currently has a best photovoltaic conversion efficiency of 9.2 % [2] (12.6% as the toxic, more expensive, and less abundant selenium-containing CZTSSe [3]).

The efficiency of CZTS cells must be approximately doubled if they are to be adopted commercially. In order to do so, the low open-circuit voltage, V_{OC}, commonly reported (~0.5, cf. ~0.7 for CIGS [4]) must be increased. Common point defects with relatively deep energy levels, such as the Cu_{Zn} and Zn_{Cu} antisites, and electrostatic potential fluctuations due to them, are likely to be limiting this [4,5]. Therefore a better understanding of such defects and cation disorder within the crystal structure in general are needed.

II. CZTS Crystal Structure

CZTS can be found in several crystal structures (all illustrated in Fig. 1 and described in Table 1): kesterite ($I\bar{4}$), stannite ($I\bar{4}2m$), PMCA (primitive mixed CuAu-like, $P\bar{4}2m$), and, at high temperatures, sphalerite (also called zinc blende, $F\bar{4}3m$). Additionally, a 'disordered kesterite' phase ($I\bar{4}2m$) has been observed, in which the Cu and Zn atoms in the z=¼ and ¾ planes of the kesterite structure (the 2*c* and 2*d* Wyckoff positions) are randomly distributed, with full Cu occupancy remaining in the z=0 plane (the 2*a* position). Kesterite is the most stable structure [6], closely followed by stannite (enthalpies of formation -359.9 and -361.9 $kJ \cdot mol^{-1}$ respectively [7], a difference of around 3 meV per atom [8]); hence the structure within a sample is often not well defined, with kesterite and stannite phases having been found intermixed. This mixing leads to variations in the band gap of the order 100 meV [9], which could contribute to limiting the low open-circuit voltage observed in CZTS cells.

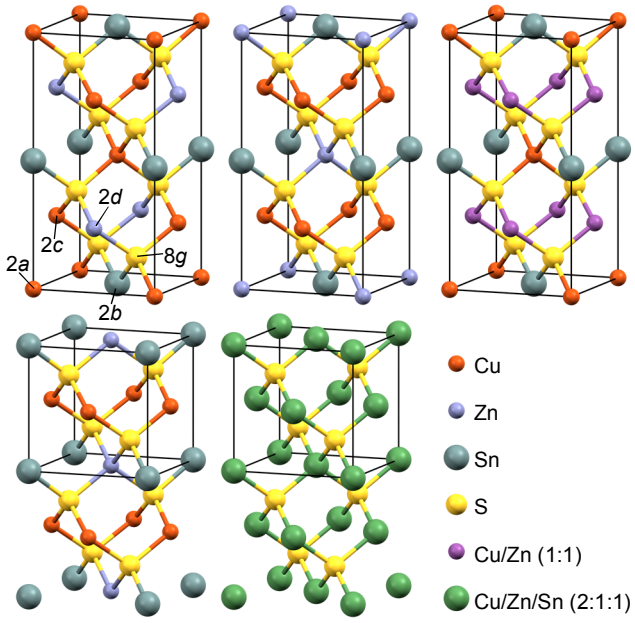

Fig. 1. Possible crystal structures adopted by CZTS. Left-to-right: kesterite (with Wyckoff sites labelled), stannite, disordered kesterite, PMCA (primitive mixed CuAu-like), and sphalerite.

Crystal structure	Space group	Wyckoff label	Atomic position	Elements
Kesterite	$I\bar{4}$ No. 82	2*a*	(0, 0, 0)	Cu
		2*b*	(0, 0, ½)	Sn
		2*c*	(0, ½, ¼)	Cu
		2*d*	(0, ½, ¾)	Zn
		8*g*	(x, y, z)	S
Stannite	$I\bar{4}2m$ No. 121	2*a*	(0, 0, 0)	Zn
		2*b*	(0, 0, ½)	Sn
		4*d*	(0, ½, ¼)	Cu
		8*i*	(x, x, z)	S
Disordered kesterite	$I\bar{4}2m$ No. 121	2*a*	(0, 0, 0)	Cu
		2*b*	(0, 0, ½)	Sn
		4*d*	(0, ½, ¼)	Cu + Zn
		8*i*	(x, x, z)	S
PMCA	$P\bar{4}2m$ No. 111	1*a*	(0, 0, 0)	Sn
		1*d*	(½, ½, 0)	Zn
		2*f*	(0, ½, ½)	Cu
		4*n*	(x, x, z)	S
Sphalerite	$F\bar{4}3m$ No. 216	4*a*	(0, 0, 0)	Cu + Zn + Sn
		4*c*	(¼,¼,¼)	S

Table 1. Descriptions of the crystal structures that CZTS can adopt.

Individual cation disorder within one of these structures is expected to be primarily only between copper and zinc, i.e. Cu_{Zn} and Zn_{Cu} antisite defects, due to the large chemical and size mismatch between tin and the other two cations. Cu_{Zn} and Zn_{Cu} point defects have been shown by ab initio calculations to have very low, or even negative, formation energies (~0 and ~240 meV respectively) [10,11], and so are expected to be easily formed. This introduces antisite defect energy levels in the band gap (Cu_{Zn} 0.15 eV above the valence band edge and Zn_{Cu} 0.10 eV below the conduction band edge [12]), which act as recombination centres, reducing device efficiency.

As Cu^+ and Zn^{2+} are isoelectronic in CZTS their X-ray scattering form factors, being proportional to the number of electrons an atom has, are the same, so it is not possible to use conventional powder X-ray diffraction (XRD) to identify the structure. This can be overcome by using the different neutron scattering lengths for Cu and Zn (7.7 and 5.7 fm respectively [13]), or anomalous X-ray scattering using an absorption edge. Anomalous scattering is the variation in atomic scattering factor for energies close to an absorption edge. It is accounted for by a correction of the form $f = f_0 + f' + i{\cdot}f''$, where f_0 is the uncorrected scattering factor, f' is the change in scattering factor magnitude and f'' is a phase shift. By comparing a non-resonant spectrum with one just below an absorption edge, where f'' is large, scattering due to the respective element can be highlighted. Calculated values [14] for CZTS at the Cu, Zn, and Sn edges are plotted in Fig. 2 to illustrate the technique.

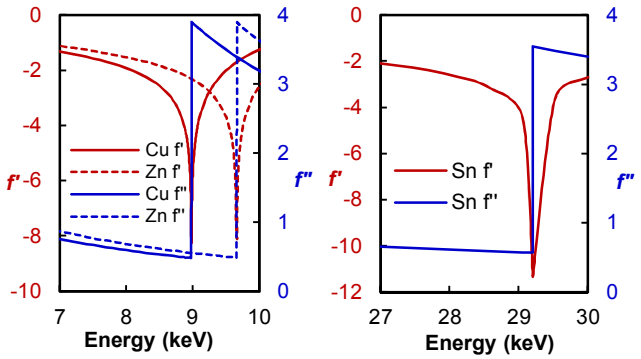

Fig. 2. X-ray anomalous scattering effects on scattering factor components. Data based on Reference [14].

Single crystal [15] and powder [16] synchrotron X-ray diffraction and neutron diffraction [17,18] have all previously been used to identify the crystal structure of CZTS and found it to be kesterite or disordered kesterite. It has also been found that as the Cu/(Zn+Sn) ratio decreases, Zn begins to substitute for Cu at the 2*a* site [16], and that Sn, the occupancy of which was investigated by synchrotron X-Ray diffraction, was found to exhibit negligible disorder for stoichiometrically correct Sn content [19].

A second order phase transition from the ordered to the disordered kesterite structure has been identified at 533 ± 10 K using Raman spectroscopy [9] and 552 ± 2 K using neutron diffraction [20], and the associated expansion of the *c* lattice parameter was observed in situ by synchrotron X-ray diffraction [21]. This implies that for usual synthesis conditions (~1070 K), the disordered structure is formed, and only during a lengthy cooling process below the critical temperature can ordering occur. This supports the observation that the Cu-Zn disordering (of the 2*c* and 2*d* sites) depends on the cooling rate after sample synthesis – 50% antisite population at each site (i.e. complete disorder) in water-quenched samples was reduced to 30% in samples with a controlled cooling rate [17].

Thus the disorder can be controlled using the cooling time below approximately 550 K. However, as it may take an impractically long cooling time to achieve a significant (>~80%) degree of order, alternative solutions such as passivation by the introduction of $[V_{Cu} + Zn_{Cu}]$ defect pairs, may be better [5]. These have been shown to aggregate with $[Cu_{Zn} + Zn_{Cu}]$ defects, reducing the structural energy and magnitude of band gap potential fluctuations, so limiting the reduction in band gap [22].

A further, first order, phase transition from the tetragonal disordered kesterite to the cubic sphalerite structure has been reported at 1149 K, with a two-phase region between 1139 and 1156 K in which both phases exist [21].

III. Experimental Details

Bulk polycrystalline samples were fabricated by solid state reaction. Finely ground Cu, Zn, and Sn powders (of manufacturer-certified purities Cu 99.9%, Zn 97.5%, and Sn 99.85%) were mixed in one alumina boat, S powder (99.5% pure, with a 30% excess to ensure full sulphurisation) was placed in another, and both were sealed together in an evacuated quartz ampoule. The ampoules were heated with a ramping rate of 5 $K \cdot min^{-1}$ to 1073 K, at which they were kept for 24 hours and then left in the furnace to cool naturally back to room temperature (over ~24 hours, at a rate ~ 0.5 $K \cdot min^{-1}$). For diffraction experiments the samples were ground to a fine powder using an agate mortar.

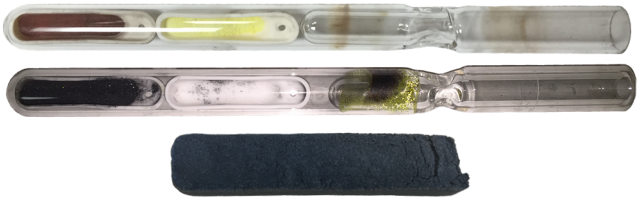

Fig. 3. Top to bottom: the elemental powders sealed in an ampoule pre-heat treatment, the ampoule post-heat treatment, and the final ingot of CZT produced

High-resolution powder neutron diffraction measurements were carried out at the HRPD beamline at ISIS. Spectra were taken at regular 10 K intervals from 4 K to 480 K.

Anomalous scattering powder X-ray diffraction experiments were carried out at Diamond Light Source. The I11 beamline was used for the Sn K absorption edge, 29.2 keV, and the I15 beamline for the Cu and Zn K absorption edges, 8.98 and 9.66 keV respectively. For the Sn edge, resonant spectra were taken precisely at the edge and comparative non-resonant spectra were taken 2 keV below it. For the Cu and Zn edges, resonant spectra were taken 10 eV below each edge and comparative non-resonant spectra at 15 keV.

Rietveld refinement was carried out using TOPAS v4.2.

SEM images, in both backscattered and secondary electron configurations, were taken using an Hitachi SU-70 FEG SEM.

IV. Results and Analysis

This paper is the first report on a comprehensive series of combined neutron and X-ray diffraction experiments on two samples with starting compositions stoichiometric and optimally doped for photovoltaic application (Cu/(Zn+Sn) = 0.8, Zn/Sn = 1.2, i.e. $Cu_{1.8}Zn_{1.2}SnS_4$). SEM images of both samples are shown in Fig. 4, illustrating the high porosity of the samples, which makes it difficult to estimate grain size.

A typical neutron diffraction pattern (for the stoichiometric sample at 4K) is shown in Fig. 5 and typical non-resonant X-ray diffraction patterns from I11 and I15 are shown in Fig. 6 and Fig. 7 respectively.

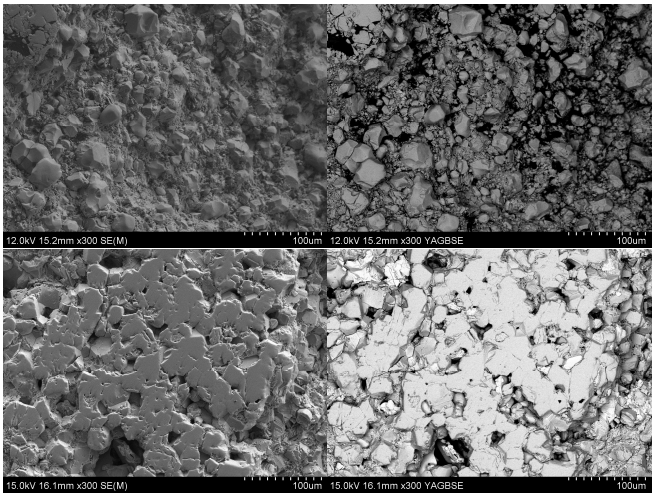

Fig. 4. SEM (secondary electron left and backscattered right) images of the stoichiometric (top) and Cu-poor, Zn-rich (bottom) samples. The scale bar is 100 μm in all images.

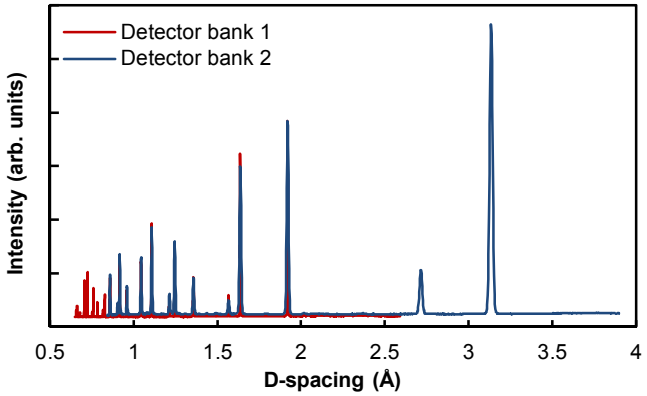

Fig. 5. Neutron diffraction pattern for the stoichiometric sample taken at 4K, showing data from the backscattering (1) and low-angle (2) detector banks at HRPD (high-angle bank data not shown).

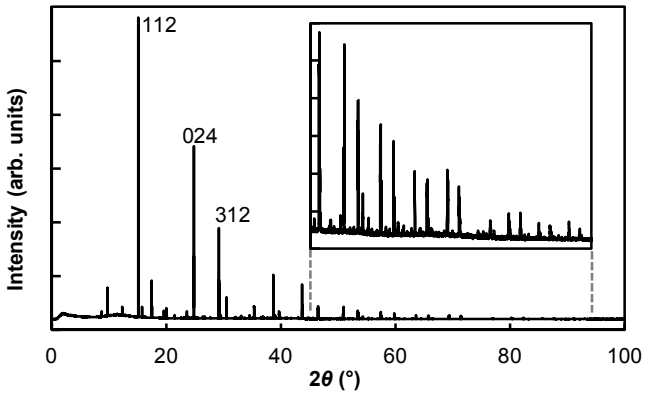

Fig. 6. X-ray diffraction pattern for the stoichiometric sample taken at room temperature using 15 keV X-rays at Diamond I11.

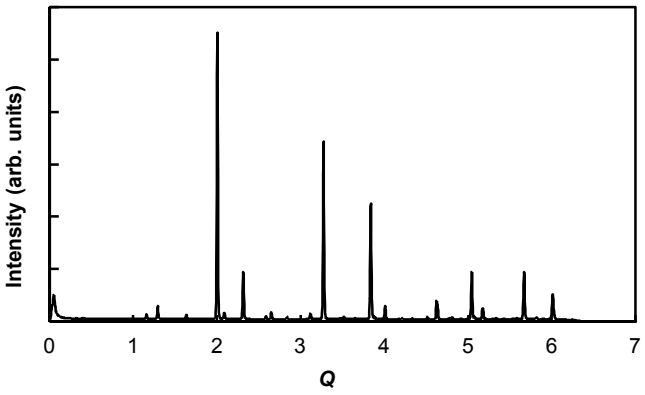

Fig. 7. X-ray diffraction pattern for the stoichiometric sample taken at room temperature using 8.98 keV X-rays at Diamond I15. $Q = 4\pi \cdot \sin(\theta)/\lambda$ is the reciprocal lattice vector.

A. Low-Temperature Crystal Structure

The crystal structure was first found without considering disorder, by Rietveld refining each possible model using 4 K neutron patterns. It is clear that both the stoichiometric and Cu-poor, Zn-rich samples are purely kesterite, with no stannite or PMCA phase present. Lattice parameters of a = 5.4299(7) Å, c = 10.836(1) Å for the stoichiometric sample and a = 5.4280(9) Å, c = 10.827(2) Å for the Cu-poor, Zn-rich one were obtained (χ^2 = 21.6 and 38.7 respectively, R = 4.1 and 3.9 respectively).

B. Cation Disorder

The I15 X-ray data, using the Sn-edge at 300 K, was used to check for tin disorder. Rietveld refinement of a model allowing Sn_{Cu}, Cu_{Sn}, Sn_{Zn}, and Zn_{Sn} occupancy showed that, in both samples, there is no tin presence on the 2*a*, 2*c*, or 2*d* sites and it fully occupies the 2*b* site (allowing for the excess Zn in the Cu-poor, Zn-rich sample). This is the result expected from previous literature.

Refinement using all other data at 300 K, allowing disorder on the 2*a*, 2*c*, and 2*d* sites, shows significant mixing of copper and zinc on all three sites. The best models of the structures of the two samples, found using neutron and all I11 X-ray data, are described in Table 2 (stoichiometric) and Table 3 (Cu-poor, Zn-rich).

Lattice Parameters	Disorder Parameters	Sulphur Positions	Quality Indices
***a*:** 5.43343(1) Å	***Cu*$_{2a}$:** 0.82(1)	***S*$_x$:** 0.2431(8)	**χ^2:** 45.8
***c*:** 10.83848(2) Å	***Cu*$_{2c}$:** 0.82(1)	***S*$_y$:** 0.2433(9)	***R*:** 12.7
	***Cu*$_{2d}$:** 0.36(1)	***S*$_z$:** 0.1282(1)	

Table 2. The best model of the stoichiometric sample from refinement of neutron, X-ray non-resonant (15 keV), Cu edge (8.97 keV), and Zn edge (9.66 keV) data at 300K.

Lattice Parameters	Disorder Parameters	Sulphur Positions	Quality Indices
***a*:** 5.43336(1) Å	***Cu*$_{2a}$:** 0.78(1)	***S*$_x$:** 0.2438(6)	**χ^2:** 42.3
***c*:** 10.83015(1) Å	***Cu*$_{2c}$:** 0.78(1)	***S*$_y$:** 0.2445(7)	***R*:** 12.2
	***Cu*$_{2d}$:** 0.25(1)	***S*$_z$:** 0.1277(1)	

Table 3. The best model of the Cu-poor, Zn-rich sample from refinement of neutron, X-ray non-resonant (15 keV), Cu edge (8.97 keV), and Zn edge (9.66 keV) data at 300K.

Despite almost all previous literature finding no disorder on the 2*a* site, these results show that the 2*a* and 2*c* sites maintain their equivalence, with equal occupancies, thus maintaining the kesterite symmetry in both samples.

It was observed during refinement of the I11 X-ray data that for the stoichiometric sample peaks were duplicated with a very small splitting ($\Delta 2\theta \sim 0.02°$). Two tetragonal phases are therefore necessary in the best model for the stoichiometric sample. Both structures being kesterite gives the best fit, which is described in Table 4. Examples of the peak splitting and improvement of the fit upon inclusion of a second kesterite phase are shown in Fig. 8. The occupancies of the two structures refine to the same value, within uncertainty, but in this model the 2*a* and 2*c* sites are no longer equal. The 2*a* site is more disordered than the 2*c* site, which is still contrary to previous literature reports. The reason for the presence of two structures is still being investigated.

Lattice Parameters	Disorder Parameters	Sulphur Positions	Quality Indices
***a*:** 5.43290(1) Å 5.43444(1) Å	***Cu*$_{2a}$:** 0.82(1)	***S*$_x$:** 0.242(1) 0.245(1)	**χ^2:** 45.8
***c*:** 10.84045(2) Å 10.83455(2) Å	***Cu*$_{2c}$:** 0.82(1)	***S*$_y$:** 0.246(1) 0.246(2)	***R*:** 12.7
	***Cu*$_{2d}$:** 0.36(1)	***S*$_z$:** 0.1282(1) 0.1285(2)	

Table 4. The best model of the stoichiometric sample from refinement of all data at 300 K. The lattice parameters and S positions are duplicated for the two distinct kesterite phases.

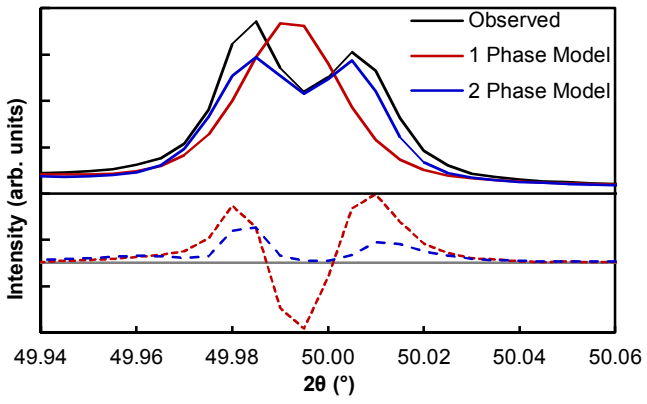

Fig. 8. An example of the improvement in fit to an I11 spectrum for the stoichiometric sample by including a second tetragonal phase.

C. *Temperature Variation*

Batch-processing was used to refine neutron patterns taken every 10 K from 10 to 480 K.

In this temperature range (below the critical temperature of the order-disorder phase transition) the thermal energy is too low to significantly change the atomic ordering on the timescale involved. As expected, for both samples, if the occupancies of the 2*a*, 2*c*, & 2*d* sites are refined for each temperature, they fluctuate unsystematically, on the scale of their uncertainty, around the best values found from the 4 K neutron pattern. Therefore the occupancies were fixed at those values to find more accurate lattice parameter variation. The sulphur position coordinates are similarly found to be constant on the scale of their uncertainty, so were also fixed.

The variation in thermal parameters, which represent the spatial broadening of atomic position due to thermal motion, for the five lattice sites is plotted in Fig. 9 (stoichiometric) and Fig. 10 (Cu-poor, Zn-rich). That the values for the 2*a* and 2*c* sites remain within their uncertainties of each other supports the conclusion that these two sites have the same occupancy.

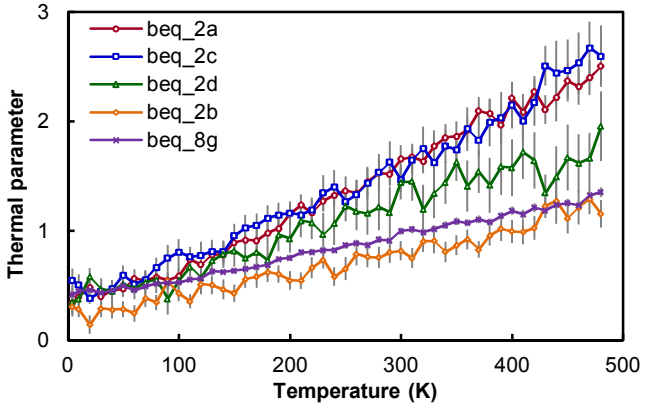

Fig. 9. The thermal parameter variation with temperature of the stoichiometric sample.

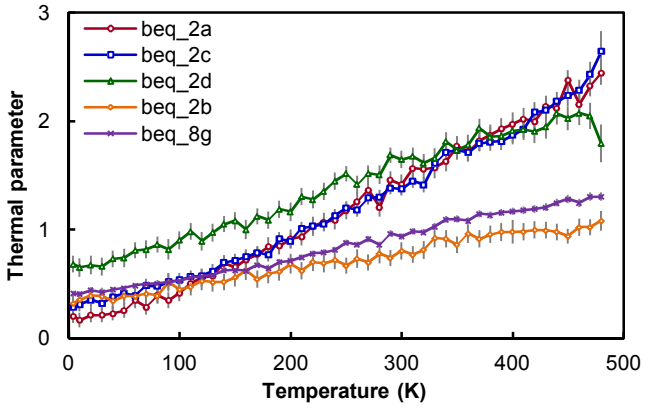

Fig. 10. The thermal parameter variation with temperature of the Cu-poor, Zn-rich sample.

The lattice parameter variation with temperature is plotted in Fig. 11 (stoichiometric) and Fig. 12 (Cu-poor, Zn-rich). As expected, the lattice parameters increase smoothly with temperature. However, below around 100 K, slight negative thermal expansion is observed for the stoichiometric sample, as is typical of such adamantine-structured materials. This will be examined in a future publication.

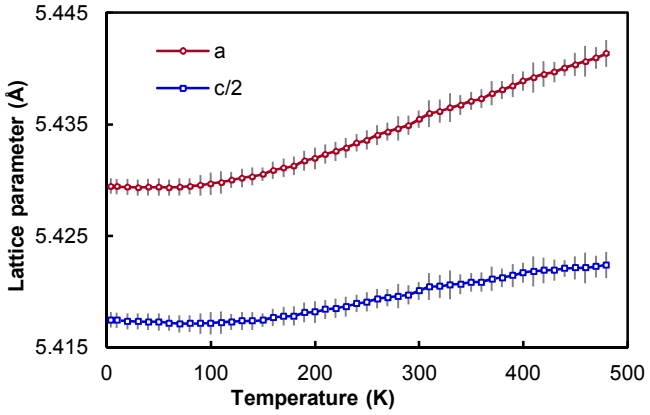

Fig. 11. The lattice parameter variation with temperature of the stoichiometric sample.

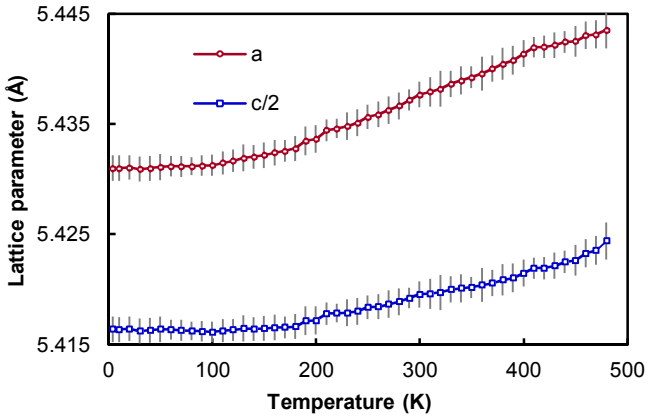

Fig. 12. The lattice parameter variation with temperature of the Cu-poor, Zn-rich sample.

V. Conclusion

Samples of CZTS with stoichiometric and Cu-poor, Zn-rich starting compositions were fabricated by solid state reaction and studied by neutron and anomalous scattering X-ray diffraction. It was found that both uniformly adopt the kesterite crystal structure, with significant cation disorder between the Cu 2*a*, 2*c*, and Zn 2*d* Wyckoff sites. This is in contrast to previous literature findings that there is usually minimal disorder on the 2*a* site. Importantly, the 2*a* and 2*c* sites were found to maintain their equivalency, thus maintaining the kesterite crystal symmetry.

In the stoichiometric sample the 2*a* and 2*c* sites were found to be 82% occupied by copper, 18% by zinc; and the 2*d* site

36% by copper, 64% by zinc. In the Cu-poor, Zn-rich sample, the 2*a* and 2*c* sites were found to be 78% occupied by copper, 22% by zinc; and the 2*d* site 25% by copper, 75% by zinc.

The appropriately lower amount of Cu_{Zn} defects in the Cu-poor, Zn-rich sample is consistent with this composition giving the best photovoltaic performance, as it results in less decreasing of the band gap and so a higher open-circuit voltage.

Two distinct tetragonal phases were identified in the stoichiometric sample. This is not yet explained.

The lattice parameters increase with temperature from 4 to 480 K as expected, except for slight negative thermal expansion of the stoichiometric sample below 100 K.

For further study and a future publication, EDX, ICPMS, and SSNMR analysis will be used to determine the post-fabrication compositions of the samples and optoelectronic study will enable the effects of crystal disorder to be quantitatively linked to material behavior relevant to photovoltaic performance.

Acknowledgement

This work was carried out with the support of the Diamond Light Source and ISIS. It would not have been possible without the assistance of the very helpful instrument scientists at HRPD at ISIS and I11 & I15 at Diamond.

References

1 Andersson, B.A. Materials availability for large-scale thin film photovoltaics. *Progress in Photovoltaics: Research and Applications* **8** (1), p.61-76, 2000, DOI: 10.1002/(sici)1099-159X(200001/02)8:1<61::aid-pip301>3.0.CO;2-6.

2 Kato, T.; Hiroi, H.; Sakai, N.; Muraoka, S.; & Sugimoto, H. Characterisation of front and back interfaces on Cu_2ZnSnS_4 thin film solar cells. *27th European Photovoltaic Solar Energy Conference,* p.2236-2239, 2012, DOI: 10.4229/27theupvsec2012-3co.4.2.

3 Wang, W. et al. Device characteristics of CZTSSe thin film solar cells with 12.6% efficiency. *Advanced Energy Materials* **4** (7), p.1301465.1-5, 2013, DOI: 10.1002/aenm.201301465.

4 Gunawan, O.; Gokmen, T.; & Mitzi, D.B. Suns-V_{OC} characteristics of high-performance kesterite solar cells. *Journal of Applied Physics* **116** (8), p.084504.1-9, 2014, DOI: 10.1063/1.4893315.

5 Scragg, J.J.S. et al. Cu–Zn disorder and band gap fluctuations in $Cu_2ZnSn(S,Se)_4$: Theoretical and experimental investigations. *Physica Status Solidi B* **253** (2), p.247-254, 2016, DOI: 10.1002/pssb.201552530.

6 Walsh, A.; Chen, S.; Wei, S.-H.; & Gong, X.-G. Kesterite thin film solar cells: Advances in materials modelling of Cu_2ZnSnS_4. *Advanced Energy Materials* **2** (4), p.400-409, 2012, DOI: 10.1002/aenm.201100630.

7 Maeda, T.; Nakamura, S.; & Wada, T. Phase stability and electronic structure of In-free photovoltaic semiconductors, $Cu_2ZnSnSe_4$ and Cu_2ZnSnS_4 by first-principles calculation. *MRS Proceedings* **1165**, p.137-143, 2009, DOI: 10.1557/proc-1165-m04-03.

8 Chen, S.; Gong, X.G.; Walsh, A.; & Wei, S.-H. Crystal and electronic band structure of Cu_2ZnSnX_4 (X=S and Se) photovoltaic absorbers: First-principles insights. *Applied Physics Letters* **94** (4), p.041903.1-3, 2009, DOI: 10.1063/1.3074499.

9 Scragg, J.J.S.; Choubrac, L.; Lafond, A.; Ericson, T.; & Platzer-Björkman, C. A low-temperature order-disorder transition in Cu_2ZnSnS_4 thin films. *Applied Physics Letters* **104** (4), p.041911.1-4, 2014, DOI: 10.1063/1.4863685.

10 Chen, S.; Yang, J.-H.; Gong, X.G.; Walsh, A.; & Wei, S.-H. Intrinsic point defects and complexes in the quaternary kesterite semiconductor Cu_2ZnSnS_4. *Physical Review B* **81** (24), p.245204.1-10, 2010, DOI: 10.1103/physrevb.81.245204.

11 Nagoya, A.; Asahi, R.; Wahl, R.; & Kresse, G. Defect formation and phase stability of Cu_2ZnSnS_4 photovoltaic material. *Physical Review B* **81** (11), p.113202.1-4, 2010, DOI: 10.1103/physrevb.81.113202.

12 Chen, S.; Walsh, A.; Gong, X.-G.; & Wei, S.-H. Classification of lattice defects in the kesterite Cu_2ZnSnS_4 and $Cu_2ZnSnSe_4$ Earth-abundant solar cell absorbers. *Advanced Materials* **25** (11), p.1522-1539, 2013, DOI: 10.1002/adma.201203146.

13 Sears, V.F. Neutron scattering lengths and cross sections. *Neutron News* **3** (3), p.26-37, 1992, DOI: 10.1080/10448639208218770.

14 Brennan, S. & Cowan, P.L. A suite of programs for calculating X‐ray absorption, reflection, and diffraction performance for a variety of materials at arbitrary wavelengths. *Review of Scientific Instruments* **63** (1), p.850-853, 1992, DOI: 10.1063/1.1142625.

15 Lafond, A. et al. X-ray resonant single-crystal diffraction technique, a powerful tool to investigate the kesterite structure of the photovoltaic Cu_2ZnSnS_4 compound. *Acta Crystallographica B* **70** (2), p.390-394, 2014, DOI: 10.1107/s2052520614003138.

16 Washio, T. et al. Analysis of lattice site occupancy in kesterite structure of Cu_2ZnSnS_4 films using synchrotron radiation X-ray diffraction. *Journal of Applied Physics* **110** (7), p.074511.1-4, 2011, DOI: 10.1063/1.3642993.

17 Schorr, S. The crystal structure of kesterite type compounds: A neutron and X-ray diffraction study. *Solar Energy Materials and Solar Cells* **95** (6), p.1482-1488, 2011, DOI: 10.1016/j.solmat.2011.01.002.

18 Espinosa-Faller, F.J. et al. Neutron diffraction and X-ray absorption fine structure evidence for local lattice distortions and aperiodic antisite substitution in Cu_2ZnSnS_4 nanoparticles. *The Journal of Physical Chemistry C* **118** (45), p.26292-26303, 2014, DOI: 10.1021/jp502150s.

19 Malerba, C. et al. Stoichiometry effect on Cu_2ZnSnS_4 thin films morphological and optical properties. *Journal of Renewable and Sustainable Energy* **6** (1), p.011404.1-12, 2014, DOI: 10.1063/1.4866258.

20 Ritscher, A.; Hoelzel, M.; & Lerch, M. The order-disorder transition in Cu_2ZnSnS_4 – A neutron scattering investigation. *Journal of Solid State Chemistry* **238**, p.68-73, 2016, DOI: 10.1016/j.jssc.2016.03.013.

21 Schorr, S. & Gonzalez-Aviles, G. In-situ investigation of the structural phase transition in kesterite. *Physica Status Solidi A* **206** (5), p.1054-1058, 2009, DOI: 10.1002/pssa.200881214.

22 Huang, D. & Persson, C. Band gap change induced by defect complexes in Cu_2ZnSnS_4. *Thin Solid Films* **535**, p.265-269, 2013, DOI: 10.1016/j.tsf.2012.10.030.